

# Lateral capacity and repair of corrosion-damaged pile bents, part 2: Numeric modeling for strength restoration

Gray Mullins, Rajan Sen, Michael Stokes, and Joseph Scott

**T**his is the second of three papers that describe the effect of corrosion damage on the lateral capacity of pile bents, the modeling and design of repair methods using fiber-reinforced polymers (FRPs), and the verification testing of a severely corroded pile bent repaired with FRPs to restore 100% of the original uncorroded pile capacity. To select a suitable FRP repair, numerical modeling was used to compare model results of unrepaired pile bents with experimental data.

## Background

Each year, corrosion damage of U.S. bridges is an expensive problem. Whereas bridges today are designed with a service life of 75 years or greater, bridges in the 1970s and earlier were more commonly expected to last only 50 years before they were replaced. In Florida, 48% of the 12,595 bridges in the state's 2021 inventory were built in the 1970s or earlier and were either nearing or well past the anticipated service life. The Florida Department of Transportation (FDOT) *Bridge Inventory 2021 Annual Report*<sup>1</sup> estimates the replacement cost for these bridges to be \$6.5 billion but notes that vigilant inspection, maintenance, and the advent of new repair technologies can extend the useful life without replacement.

Approximately one-third of FDOT bridges are over water, and these bridges make up more than 60% of all bridge deck area in the state. (Overwater bridges are longer on average than other bridges.) The most common pier configuration for overwater bridges built in the 1950s, 1960s, and 1970s was

- This is the second of three papers that highlight the effects of corrosion damage on bridge pile bents.
- The first identified the magnitude of lateral capacity loss from corrosion.
- This paper outlines numerical modeling efforts aimed at accurately assessing the degree of capacity loss from corrosion damage and recommends suitable carbon-fiber-reinforced polymer repair schemes.

a pile bent (**Fig. 1**). Pile bents are described as driven piles aligned in rows that extend up from the bearing soil to the underside of the bridge at the location of a pile cap. The pile cap is cast around the piles to form a support beam for the superstructure elements. Pile-bent-type piers are inexpensive to build, but they are vulnerable to splash-zone-related corrosion damage due to tidal-fluctuation-induced cycles of wetting and drying.

The splash zone produces high surface chloride concentrations, oxygen, and moisture, which are the cornerstones of a corrosive environment. Within the splash zone, chloride contamination is greatest in the region 1.68 m (5.51 ft) above the highwater elevation. This region (herein referred to as the damage zone) is where most corrosion damage occurs. Seawater spray and evaporation in this zone contribute significantly to the ingress of chlorides from the surface of the concrete to the steel reinforcement, especially on structures with preexisting cracks.<sup>2</sup>

The reduction in cross section of the steel reinforcement from corrosion results in a loss in bending capacity; axial capacity is less affected unless the concrete cover spalls. Depending on the maintenance strategy of the owner, repairs may be made after the onset of visible corrosion cracks or after significant steel loss, spalling, and missing concrete cover. Numerous repair techniques to mitigate corrosion damage have been explored. One method involves wrapping the piles with epoxy- or urethane-saturated structural fiber meshes. **Figure 2** shows preemptive FRP confinement of piles in Biscayne Bay, Fla., after the onset of visible cracks. FRP wraps are high-strength, lightweight, and durable materials and are ideal to withstand expansive forces caused by the corrosion of steel reinforcement.

In addition, these materials can restore lost flexural capacity.<sup>3</sup> Two layers of wrap have been shown to provide the most efficient seal to prevent further moisture, oxygen, and chloride ingress and significantly reduce corrosion rates.<sup>4</sup>

Unfortunately, unless the concrete cover is dislodged before a repair to expose the amount of remaining steel reinforcement, the residual structural capacity of the piles is uncertain. The first paper in this series<sup>5</sup> showed that 10% steel loss had negligible effects on the lateral capacity of pile bents (1% loss), and the piles had visible but narrow longitudinal cracks (with maximum widths of 0.5 mm [0.02 in.]). Pile bents with 30% steel loss had wider cracks (1.5 mm [0.06 in.] maximum) and lost 24% of their lateral capacity; pile bents with 50% steel loss had even wider cracks (3 mm [0.1 in.] maximum) and 30% loss in lateral capacity. Where concrete cover is completely dislodged, greater than 50% steel loss can be assumed; however, the correlation between average steel loss and crack widths presented here does not indicate the local conditions of the steel, which can be many times worse than the correlation might imply. Nevertheless, when designing a repair using FRP wraps with transversely oriented fibers to stave off further corrosion damage, the designer can use additional longitudinally aligned fibers to bolster bending resistance or replace missing steel reinforcement in piles.

## Objectives and scope

This paper presents a study that used numerical modeling to compare the lateral capacities of a severely corroded pile bent repaired with carbon-fiber-reinforced polymers (CFRPs) and an identical uncorroded pile bent. In previous studies,<sup>5-7</sup> accelerated corrosion techniques were used to simulate typical



**Figure 1.** Typical pile bent built in the 1970s. This example is from the Alligator Alley stretch of southbound Interstate 75 in southern Florida between Naples and Fort Lauderdale.



**Figure 2.** Fiber-reinforced polymer confinement applied from cap to mudline to arrest corrosion-induced crack growth.

field conditions for damaged piles. One-third-scale model pile bents with corrosion damage were laterally loaded to demonstrate the effects of up to 50% steel loss. The objective of this phase (part 2) of the test program was to develop a viable CFRP repair capable of fully restoring the original uncorroded strength of the pile bent to the damage zone where 100% of the steel is assumed to have corroded away.

## Approach

The methodology adopted to design a repair and restore the original lateral capacity of the model pile bent involved the development and calibration of numerical models to assess the residual strength of corrosion-damaged pile bents. Model results were compared with experimental test results for verification. The model was then used in conjunction with verification calculations to determine the amount of CFRP materials required to restore the lost capacity, assuming no prestressing steel remained. Weaker FRP materials were not considered because they would have required an excessive amount of fabric material (fibers) to provide a satisfactory repair.

## Numerical modeling

To provide a reliable pile repair scheme, the laboratory testing setup for the five-pile bents presented in part 1<sup>5</sup> of this paper

series was numerically modeled and verified to be representative of the laboratory test results. Numerical models of the lab-tested pile bents presented in part 1 were developed to match the percentages of steel loss within the damage zone in the lab specimens: 0% (control), 10%, 30%, and 50%. Values of concrete strength, modulus, and levels of prestress were adjusted to calibrate the model parameters. Using the calibrated model, CFRP material was then added to the surface of the numerically modeled piles to determine an acceptable amount of longitudinal carbon fibers.

## Pier geometry

The pier geometry and material properties used for the original test program<sup>5-7</sup> were input into nonlinear finite element software that is commonly used for modeling the lateral response of bridge piers. The same software was used to model prototype bridges in part 1 of the study to determine the in-service bending moment distribution in pile bents.<sup>5</sup> The dimensions of the laboratory-tested pile bents are briefly described here. Complete details can be found in the original test program.<sup>5-7</sup>

Each pile bent was composed of five 152 mm (6.00 in.) square prestressed concrete piles. These piles were 3.4 m (11 ft) long, spaced at 1 m (3.3 ft), and embedded 102 mm

(4.00 in.) into a pile cap measuring  $0.3 \times 0.3 \times 4.6$  m ( $1 \times 1 \times 15$  ft). The base of each pile was embedded 203 mm (8.00 in.) into an identical  $0.3 \times 0.3 \times 4.6$  m floor-level beam anchored to the laboratory strong floor (Fig. 3). This resulted in a 3 m (10 ft) clear pile length from the bottom of the pile cap to the point of fixity. The focus of the test setup was to simulate the upper half of the pile moment diagram, which included the chloride-rich damage zone. This region of the moment diagram extended from the bottom of the pile cap down to the inflection point (zero moment)  $10D$  below, where  $D$  is the pile size. The actual prototype moment diagram would be the same above the inflection point, but the point of fixity below the inflection point would be far below the mudline (much greater than  $10D$ ), depending on the lateral soil stiffness. Each of the five 3.4 m long piles was cast with 279 mm (11.0 in.) of uncontaminated concrete at the top, followed by 559 mm (22.0 in.) of chloride-contaminated concrete at the damage zone above high water, with uncontaminated concrete used for the remaining pile length.

All pile-bent components were included in the numerical models down to the floor-level beam so that a direct comparison to laboratory load responses could be made. For the numerical model, each pile was broken into segments to represent variations in concrete strength, effective prestress, and area of the steel strands along the length of the pile.

## Chloride-contaminated concrete

A change in concrete strength in the physically tested one-third-scale pile bents<sup>5-7</sup> was the byproduct of the 3% chloride added to the FDOT Class V concrete to contaminate the damage-zone regions. When casting the piles, the concrete for the undamaged portions of the piles was placed first and thin sheet metal separators were used to prevent the concrete from flowing into the damage-zone regions in the casting bed. Then a chloride additive was mixed into the concrete in the same truck, and the chloride-contaminated concrete was quickly placed in the damage zone. The sheet metal separators were removed, and the concrete was vibrated and finished. The chloride additive is intended to act as a curing accelerator, but in this case, the additional chloride-rich fluid ( $53 \text{ L/m}^3$  [ $11 \text{ gal./yd}^3$ ]) also increased the water-cement ratio. As a result, where the uncontaminated concrete had a 28-day strength of 59 MPa (8.6 ksi), the chloride-contaminated regions were only 38 MPa (5.5 ksi), which met the minimum specified strength. In hindsight, perhaps two different trucks could have been deployed for mixing, but the accelerator could not have been added at the batch plant due to the short working time (approximately 20 minutes). It is also unclear whether the remaining uncontaminated water volume would have been sufficient to initiate mixing while the truck was in transit to the site where the remaining fluid additive would have been added. Regardless, numerical modeling incorpo-

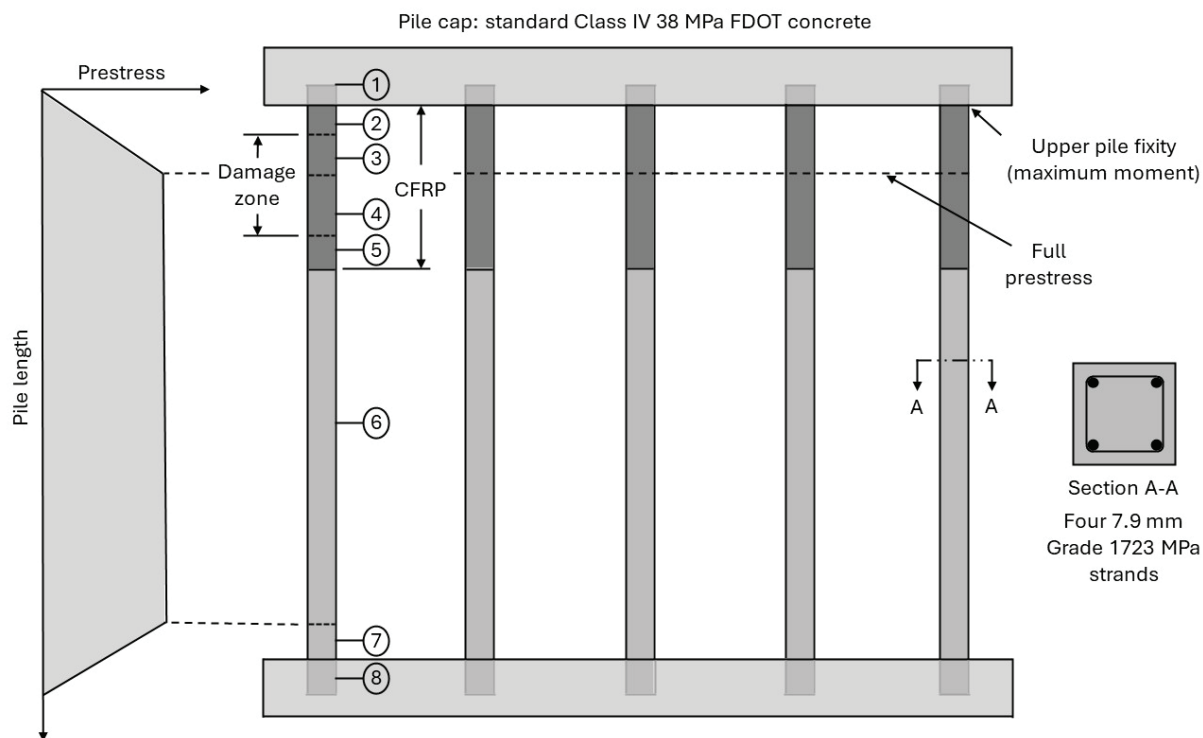


**Figure 3.** Pile segments used in numerical models to account for changes in concrete and effective prestress. Note: CFRP = carbon-fiber-reinforced polymer; FDOT = Florida Department of Transportation.

rated the as-built parameters to allow direct comparisons with the laboratory-measured response to lateral loading.

## Transfer length considerations

Prototype FDOT bridge piers (replicated by the laboratory one-third-scale bridges) used 0.3 m (1 ft) pile-to-cap embedment lengths.<sup>5-7</sup> FDOT section 3.5.1 denotes this arrangement as a pinned connection;<sup>8</sup> however, the tests presented in part 1 of this paper series showed that an appreciable amount of fixity was exhibited; hence, this connection was not pinned.<sup>5</sup> The point of upper pile fixity (just below the cap) was 102 mm (4.00 in.) from the top end of the pile and was not far enough from the end to transfer the full level of prestress to this critical moment location (Fig. 3). Values vary in literature for transfer length (for example, from  $50d$  to  $100d$ , where  $d$  is the diameter of the strand). In this investigation, a lower value of  $50d$  (410 mm [16.1 in.]) was assumed. That value had been measured in a previous study using the same type of piles and concrete.<sup>9</sup> The numerical model incorporated this effect by breaking each of the piles into a minimum of eight segments and applying the average effective prestress to each segment, assuming a linear increase from zero at the ends to full prestress at the transfer length (Fig. 3). **Table 1** shows the average effective prestress in each of the eight segments and

concrete strength variations from the top segment (segment 1) through the bottom segment (segment 8) in the piles with 0% steel loss (controls). Segment 5 was included to accommodate the CFRP shear lap length required to develop the carbon fibers (discussed later).

The effective prestress in the steel in the damage zone was changed slightly for the pile bents with corrosion damage. The initial prestressed concrete strain is only about  $-200 \mu\epsilon$ , whereas the strain in the strands from the initial effective prestress level is closer to  $+5200 \mu\epsilon$ . Changes in the concrete and steel stresses are linked by the same change in strain. Hence, as the concrete expands and relaxes down to 10% of the original prestress (from  $-200$  to  $-20 \mu\epsilon$  caused by 90% steel section loss), the strand simultaneously elongates, causing a stress increase of 3% ( $180 \mu\epsilon / 5200 \mu\epsilon$ ). However, the force in the steel is more affected by the dramatic cross-sectional loss than it is by the slight increase in stress. **Table 2** summarizes the loss of concrete prestress used in the models caused by steel corrosion and cross-sectional losses.

## Damage model results

The numerical models were run numerous times to calibrate the material properties of the concrete. Specifically, the

**Table 1.** Modeled pile segment values (no corrosion control bent)

Segment	Length, mm	$f'_c$ , MPa	Effective prestress, MPa
1 (in cap)	102	59	129
2 (above damage)	203	59	485
3 (damage zone)	203	38	927
4 (damage zone)	356	38	1035
5 (develop CFRP)	177	59	1035
6 (normal)	1930	59	1035
7 (above base)	203	59	776
8 (in base)	203	59	259

Note: CFRP = carbon-fiber-reinforced polymer;  $f'_c$  = compressive strength of concrete. 1 MPa = 0.145 ksi.

**Table 2.** Damage-zone model input prestress values

Loss, %	Concrete $\Delta$ , MPa	Steel $\Delta$ , MPa	Concrete compressive stress, MPa	Steel tensile stress, MPa	Concrete force, kN	Steel force, kN
0	0	0	6.9	1034	159	159
10	-0.7	4.3	6.2	1039	144	144
30	-2.0	12.9	4.9	1047	112	112
50	-3.4	21.8	3.5	1056	81	81
90	-6.2	39.9	0.72	1074	17	17

Note:  $f'_c$  = compressive strength of concrete;  $\Delta$  = change in stress. 1 kN = 0.225 kip; 1 MPa = 0.145 ksi.

modulus of elasticity was swept through a range of acceptable values. Section 19.2.2 of the American Concrete Institute's *Building Code Requirements for Structural Concrete (ACI 318-14) and Commentary (ACI 318R-14)* states that "the modulus of elasticity for concrete is sensitive to the modulus of elasticity of aggregate and mixture proportions of the concrete. Measured elastic modulus values can range from 80 to 120 percent of calculated values."<sup>10</sup> Initial stiffness of the modeled load-displacement response of the pile bents showed that an increase in modulus of 20% yielded the closest match to the experimental results. **Figure 4** shows the load-displacement response from the laboratory-tested and modeled pile bents for no damage and 50% steel loss. Not shown are findings from the 10% and 30% steel-loss tests. No appreciable change was observed at 10% steel loss, and the numerical model results for 30% steel loss agreed with measured test results. Complete details of the model-versus-measured results can be found elsewhere.<sup>11</sup>

In addition, a model was run with 99.9% steel loss (called 100% in Fig. 4). The 0.1% remaining steel was required to satisfy software input parameters, but it provided no appreciable contribution to the capacity. The service load (44 kN [9.9 kip] per pile) effectively simulated approximately 28% of the original prestress force offered by the uncorroded strands (1.6 MPa [232 psi]) and maintained some lateral capacity even when all steel was missing.

Interaction diagrams for each of the pile segments were generated using calculations based on nominal axial and bending capacities. The nonlinear finite element software generates

interaction diagrams, but the program incorporates reduction factors, which in some cases can be outdated. For the calculated interaction diagrams presented herein, these design resistance factors were intentionally excluded to obtain values that would be a better representation of what could be measured in an experiment. **Figure 5** shows the contribution of the service load to the pile bending capacity. Typically, foundation elements in overwater bridge piers are loaded to only 10% of the ultimate axial resistance where bending resistance controls the design.

At 100% steel loss, no appreciable bending resistance can be developed unless axial load is applied to offset the tensile stresses (Fig. 5). As expected, at lower bending stresses, a loss in prestress results in an increase in axial resistance. At the service-level axial load, the bending resistance in the undamaged region just below the cap (with reduced effective prestress) is similar to that below the damage zone (full effective prestress). Both of those regions had the higher-strength concrete, and both retained 100% steel cross sections in all tests. In fact, it is likely that the modeled bending capacity just below the cap will never be affected by the loss in effective prestress at typical axial load levels for bridge piers. **Table 3** lists the bending resistance from Fig. 5 for all modeled pile segments at the service-level axial load.

### Repair calculations

The calibrated model agreement (Fig. 4) provided the confidence to proceed with the assessment of a viable CFRP repair model of the corrosion-damaged pile bent, but first, prelim-

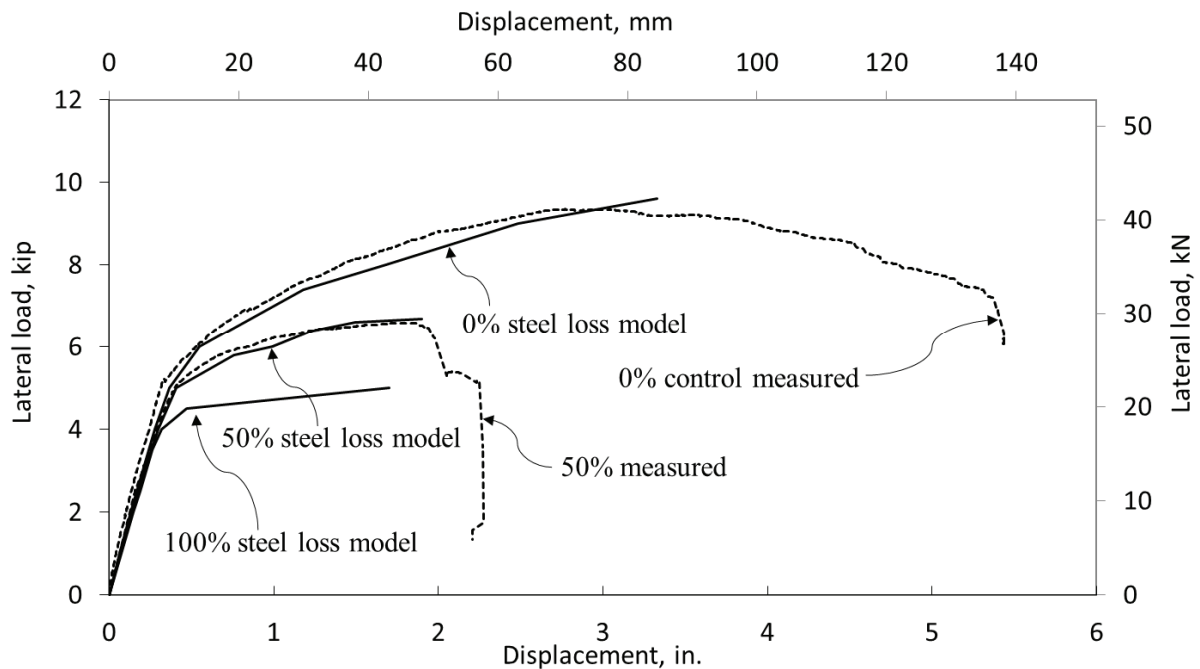


**Figure 4.** Modeled versus measured pile bent response to lateral loading. 1 mm = 0.0394 in.; 1 MPa = 0.145 ksi.

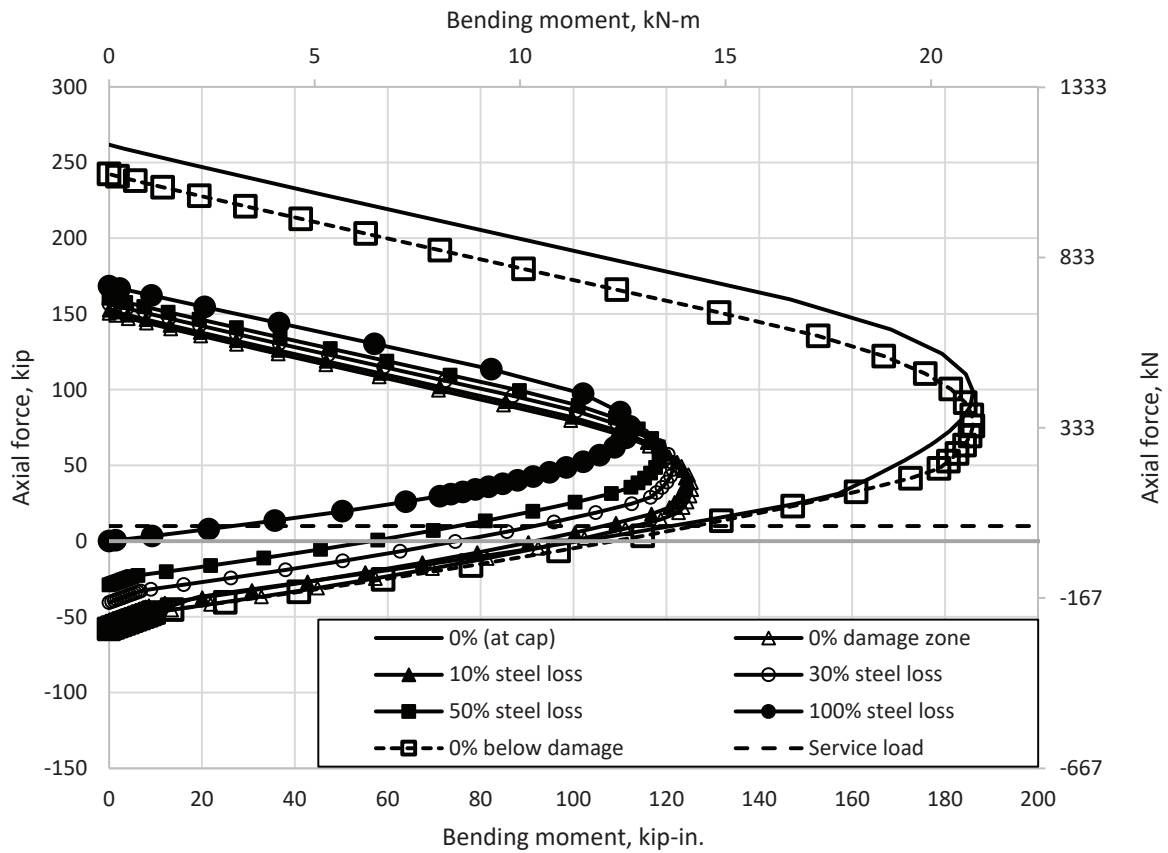


**Figure 5.** Interaction diagram for all portions of the piles where changes in steel area and concrete strength affected capacity.

**Table 3.** Bending resistance at service-level axial load

Steel loss, %	Bending resistance at service load, kN-m	$f'_c$ , MPa	Loss in bending resistance, %
0 (at cap)	13.7	59	4
0 (damage zone)	12.8	38	10
10	12.0	38	16
30	10.4	38	27
50	8.5	38	40
100	3.0	38	79
0 (below damage)	14.3	59	0

Note:  $f'_c$  = compressive strength of concrete. 1 m = 3.281 ft; 1 kN = 0.225 kip.

inary calculations were performed (without finite element modeling) to determine how many longitudinal layers would be necessary to model a full-capacity restoration.

Interaction diagrams based on nominal capacities were developed where strains at the top and bottom of the pile were swept through values ranging from the maximum compressive strain of the concrete (-0.003) to the rupture strain of the CFRP

repair material (0.0162). Any confinement benefits that might result from an outer spirally wrapped layer were not taken into account; however, the effect of an estimated dead load on the piles at the time of repair was considered. This load was applied only to the concrete core because the repair material (new concrete cover and CFRP wrap) would normally be applied in the field under a zero-stress condition while the core is precompressed under dead loads. Cured laminate properties

for a commercially available CFRP fabric and epoxy system were used in the calculations. This product has a design tensile strength of 1056 MPa (153.2 ksi), elastic modulus of 64.9 GPa (9410 ksi), and an in-place strength of 1.06 kN/mm of width per layer (6.1 kip/in. of width per layer).

**Figure 6** shows the interaction diagrams for an undamaged cross section, a damaged cross section with 100% steel loss, and a damaged cross section repaired with one layer of CFRP. With 100% steel loss and associated loss in concrete precompression, the damaged cross section gains a slight increase in axial compressive capacity while losing all axial tensile capacity from the steel. With the addition of one layer of CFRP, the repaired interaction diagram fully envelops the undamaged diagram, thereby showing that at any axial force, the bending capacity of the repaired section meets or exceeds that of an undamaged pile. At zero axial force, the pure bending capacity is increased to 16.6 kN m (147 kip in.), which is approximately 28% higher than the pure bending capacity of an undamaged cross section. Also, the characteristically high tensile strength of the CFRP increases the axial tensile capacity by 152% and moves the balanced point on the interaction diagram (the point at which concrete crushes and CFRP ruptures) below the x axis into the region of net axial tension. Once these calculations gave confidence that one longitudinal layer of CFRP would be sufficient to fully restore the capacity of the undamaged pile, finite element modeling of this repair

was conducted to determine the lateral load versus lateral displacement response for the five-pile bents.

## Repaired pile model results

The same cured laminate properties used in the preliminary calculations were used to numerically model a carbon-fiber shell around the damaged piles. The nominal CFRP fabric thickness is 1 mm (0.04 in.), but it was modeled using the equivalent area of circular reinforcement bars (an option for additional mild steel), where 120 carbon-fiber strands measuring 1.3 mm (0.051 in.) in diameter were placed at the outer edges of each pile face (**Fig. 7**). Manufacturer values for the CFRP tensile strength and modulus were input in place of the mild steel values.

CFRP was modeled to cover segments 2 through 5 (Table 1), and the strand area in Fig. 7 varied. Segments 2 and 5 on either side of the damage zone provided bonded development length for the carbon fibers and retained 100% of the steel section. Segments 3 and 4, representing the damage zone, had no steel.

Model results show a significant increase in tensile and bending resistance in those regions with the CFRP wrap. A more modest increase in compression resistance also occurred. **Figure 8** shows the effects of the CFRP material on the calculated interaction diagrams for three segment types:

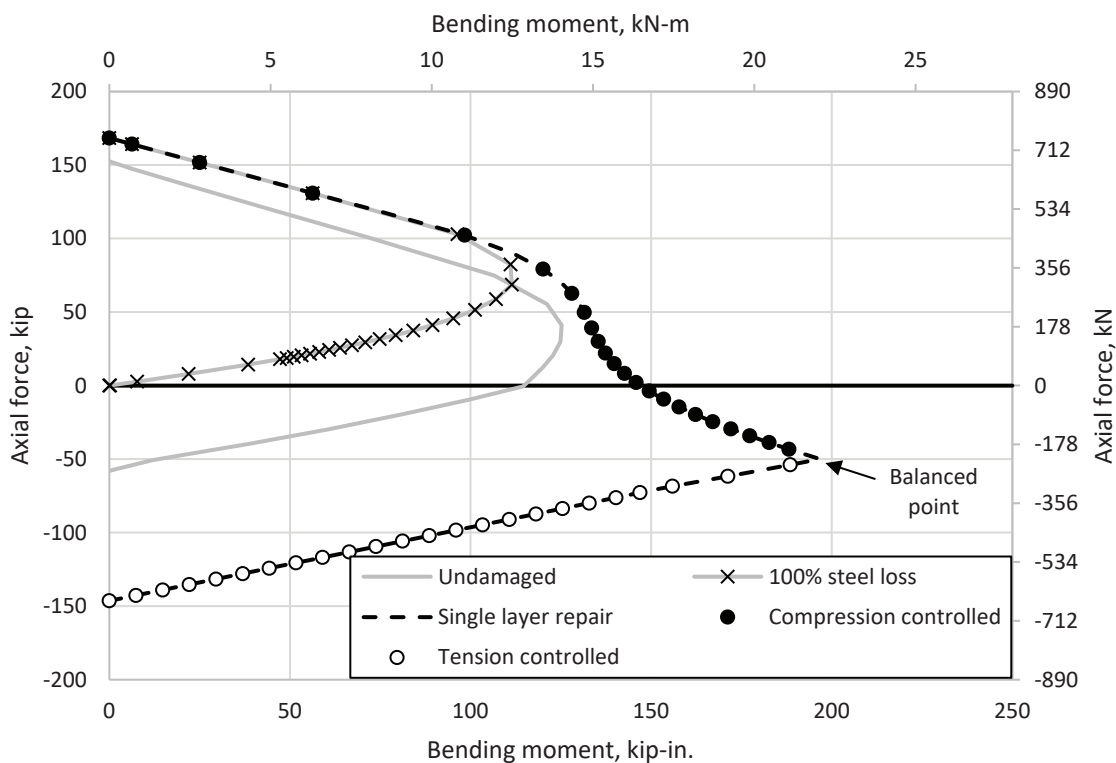


**Figure 6.** Interaction diagrams for an undamaged section, a section with 100% steel loss, and a section with 100% steel loss that has been repaired with one layer of carbon-fiber-reinforced polymer.

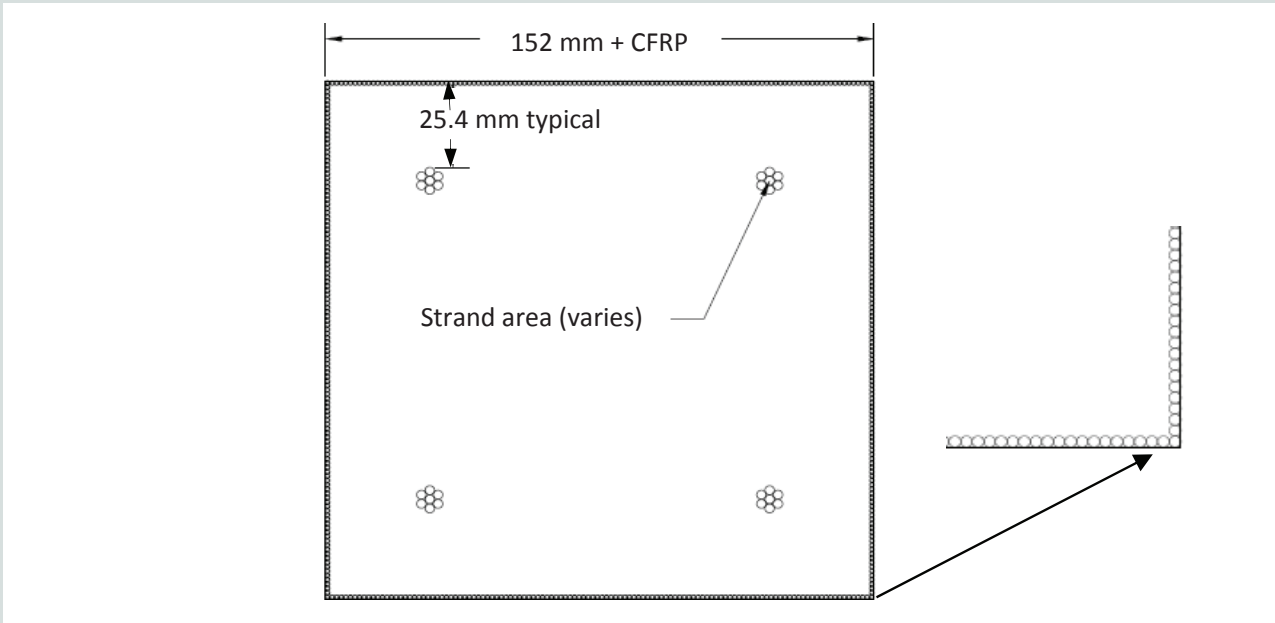


**Figure 7.** Modeled pile cross section with carbon-fiber-reinforced polymer (CFRP) wrap. Note: 1 mm = 0.0394 in.

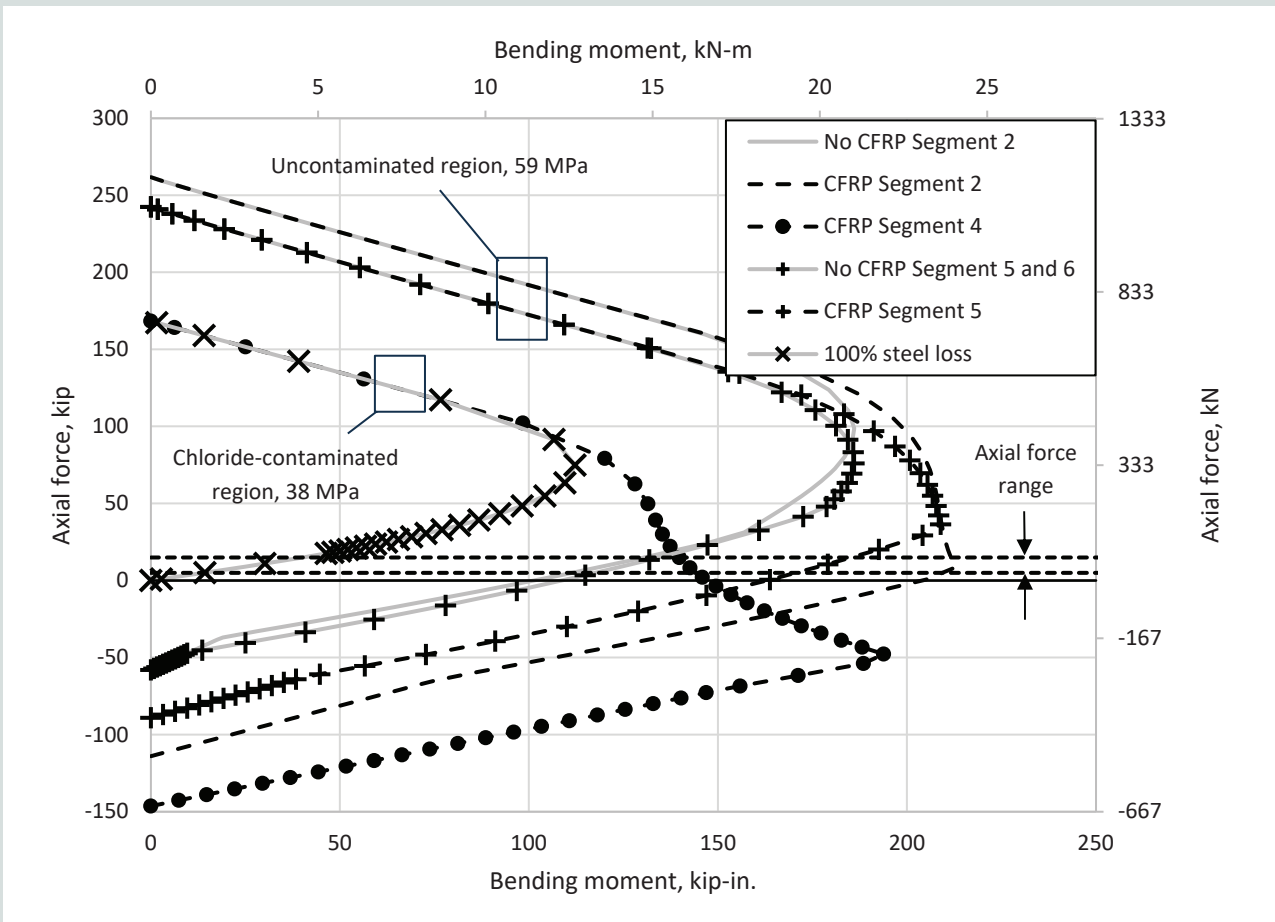


**Figure 8.** Interaction diagrams for pile segments with and without carbon-fiber-reinforced polymer (CFRP) repair material.

- 100% steel loss in the damage zone (segment 4)
- the undamaged region below the cap (segment 2)
- the undamaged regions below the damage zone (segment 5)

In all cases, the dashed line is the CFRP-repaired segment. Three limit states were used in the calculations to define nominal capacity:

- concrete crushing
- steel rupture
- CFRP rupture

The compression-controlled regions of all segments were defined by concrete crushing. It is important to recall the difference between the concrete compressive strength of pile segments contaminated with chloride and those with uncontaminated concrete. This explains the large disparity between the axial force intercepts (zero bending moment) of the interaction diagrams for segments 4 and 5. The axial force intercepts for segments 2 and 5 only differ because prestressing is not fully developed in segment 2. The tension-controlled regions were defined based on whether steel remained in the cross section. Because segment 4 experienced 100% steel loss, its nominal capacity was defined by concrete crushing and CFRP rupture. Segments 2 and 5 contained all three materials, but the tension-controlled regions of the interaction diagrams were limited by rupturing of the steel strands. As noted previously, segment 5 was added to the model to provide shear-bond development below the damage region but segment 5 is otherwise the same as segment 6. Due to the portal frame response of the lateral loading, the axial

load increases in the leading piles and decreases in the trailing piles, so the range of axial loads in any of the five piles is also shown as two dotted lines. Although segment 4 had concrete with a lower compressive strength than that of segments 2 and 5, one layer of CFRP is sufficient to provide a bending capacity higher than that of an undamaged pile within the axial load range. **Table 4** shows the axial loads in all five piles for lateral loads up to failure as predicted by the model. The axial loads in the center piles agree with portal frame analysis predictions where no change occurs while a linear/elastic response was observed (up to 18 kN [4.0 kip] lateral load).

Software output indicated concrete cracking (Table 4) in various pile segments beginning in load step 3; segment 3 was the first to crack, followed by segments 4, 2, and then 5. As discussed, segments 3 and 4 were composed of the low-strength concrete but were in lower moment regions than segment 2, which had higher-strength concrete beneath the cap. Segment 5, located below the damage zone, registered cracking only after extreme deformations; however, concrete cracking within the CFRP regions did not cause failure, which in this case was defined by model instability or an inability to balance forces within the finite element model.

When modeling these types of repairs, it is necessary to recognize that there is an infinitesimally small region between the pile cap and the top of the CFRP wrap that is unaffected by repair material. Regions of this type can only develop the bending resistance of the original unrepaired/undamaged section. Table 3 notes that this cross-section type has a bending resistance of 13.7 kN m (121 kip-in.) at the original service load prior to lateral loading. For the range of axial loads in all piles (23 to 70 kN [5.2 to 16 kip]) shown in Table 4, the bending resistance in this region during lateral loading cannot exceed 14.9 kN-m (132 kip-in.), so where

**Table 4.** Axial load in each pile versus applied lateral load

Lateral load, kN	Pile 1 axial load, kN	Pile 2 axial load, kN	Pile 3 axial load, kN	Pile 4 axial load, kN	Pile 5 axial load, kN	Segments cracked
4	43	44	44	45	46	None
9	41	44	44	45	48	None
13	39	44	44	45	50	3
18	37	44	44	45	52	3 and 4
22	38	44	45	46	54	3, 4, and 2
27	37	45	47	50	59	3, 4, and 2
31	34	42	45	48	59	3, 4, and 2
36	34	44	47	50	60	3, 4, and 2
40	33	43	47	51	62	3, 4, and 2
44	30	42	47	53	66	3, 4, and 2
52	23	40	47	55	70	3, 4, 2, and 5

Note: 1 kN = 0.225 kip.

the interaction diagram at service axial load for the CFRP-wrapped segment 2 (Fig. 8) shows bending resistance of 24 kN-m (210 kip-in.), an upper limit must be applied at the pile-to-pile cap interface that is no greater than the bending resistance of the undamaged, unwrapped pile. The model in this case assumed the strength of CFRP-repaired segment 2 extended into the cap and therefore overpredicted the pile bending resistance at the pile-to-cap interface.

By looking at the modeled bending moment beneath the cap in each pile as load was progressively increased (Table 5), the undamaged, unwrapped bending resistance (14.9 kN-m [132 kip-in.]) can be used as a limit and provide a more realistic lateral pile-bent capacity. The result is a lateral pile bent capacity between 40 and 44 kN (9 and 9.9 kip), where all piles exceeded the limiting bending moment. Figure 9 shows the measured response to lateral loading for the undamaged control pile bent (no steel loss) from part 1 of this testing program.<sup>5</sup> This figure also shows the predicted numerical model response both with and without the upper limit for the bending resistance. The maximum lateral-load cutoff was established by rerunning the model with finer load increments to identify when at least three out of the five piles failed. This rationale was based on part 1 findings, where simultaneous failure in three of five piles occurred in one of the tested pile bents.

## Discussion

From a practical perspective, when planning a repair using CFRP or any other type of FRP, the designer must consider the lap lengths required to transfer the fiber forces into the existing concrete substrate. This consideration is similarly important for the overlap of transverse fibers used for confine-

ment. The added benefit of concrete confinement from CFRP repairs was not considered in the numerical models presented herein because the software assumed that normal confinement was provided and did not provide a means to simulate losses in spiral reinforcement. Hence, the transversely oriented fibers were assumed to replace the missing steel spiral reinforcement; however, the nonlinear finite element software provides an additional confinement option and can include the associated strength benefits in cases where CFRP confinement exceeds the original stirrup strength. Design for lost confinement from corroded stirrups should simply provide a strength in carbon fibers that is equivalent to the strength of the original transverse steel stirrups. Assumption of full steel loss is conservative, and most FRP wrap repairs include at least one layer of a spiral layup process like the one in Fig. 2.

The one-third-scale piles tested in part 1 of this testing program were, unfortunately, compromised by a high water-cement ratio resulting from the addition of the chloride-contaminated fluid additive. In this case, the unrepaired, lower-strength, chloride-contaminated regions with corroded steel cracked first despite being in a lower moment region relative to the underside of the cap. In actual field conditions, the core concrete would not be a different, weaker concrete, and modeling the repair would require fewer pile segments.

The properties of CFRP repair materials vary among suppliers, but all are published and can be easily input to predict the effectiveness of a repair scheme. The fabric selected for the one-third scale piles was also used to demonstrate how a standard array of pile sizes can be similarly repaired with CFRP (Fig. 10, 11, and 12). Where the Fig. 6 results showed one layer was more than adequate for the 152 mm (6.00 in.) piles, larger piles require more CFRP layers to offset changes in the ratio

**Table 5.** Model-predicted internal bending moments beneath the cap

Lateral load, kN-m	Pile 1 axial load, kN-m	Pile 2 axial load, kN-m	Pile 3 axial load, kN-m	Pile 4 axial load, kN-m	Pile 5 axial load, kN-m
4	1.5	1.5	1.5	1.5	1.5
9	3.0	3.0	3.0	3.0	2.9
13	4.4	4.5	4.5	4.5	4.4
18	5.8	5.9	5.9	5.9	5.9
22	7.0	7.2	7.3	7.3	7.5
27	8.5	8.8	8.9	8.9	9.3
31	10.1	10.5	10.6	10.7	11.1
36	11.5	12.0	12.2	12.3	12.7
40*	13.1	13.6	13.8	14.0	14.5
44*	15.1	15.6	15.9	16.1	16.6
52	21.6	22.1	22.4	22.6	20.8

Note: 1 m = 3.281 ft; 1 kN = 0.225 kip.

\*Piles 3, 4, and 5 exceeded the 14.9 kN-m upper bending limit at 42 kN.

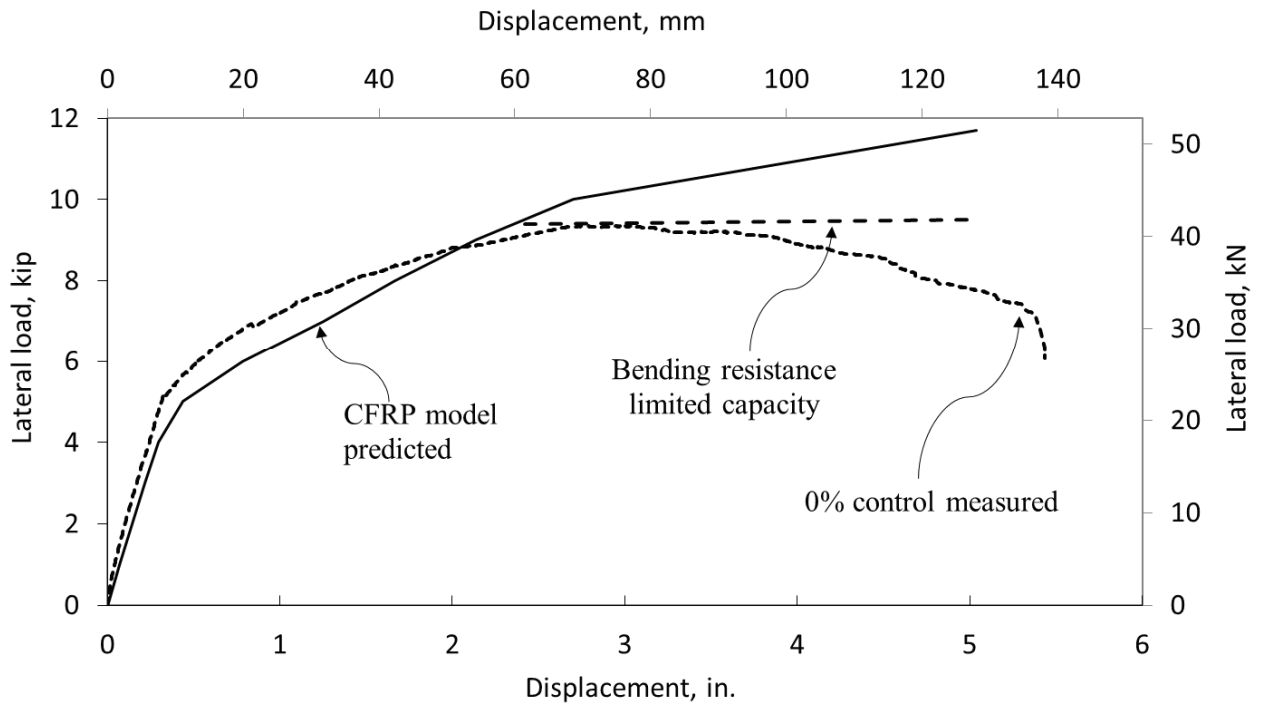


Figure 9. Model results for pile bent repaired with carbon-fiber-reinforced polymer (CFRP).

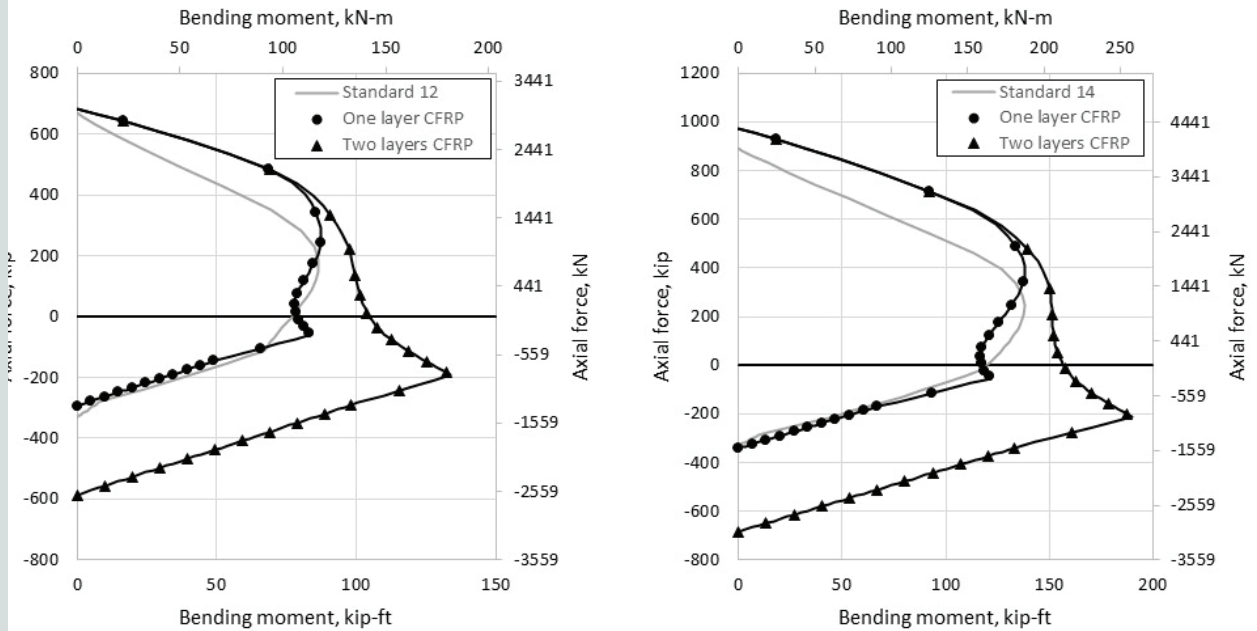
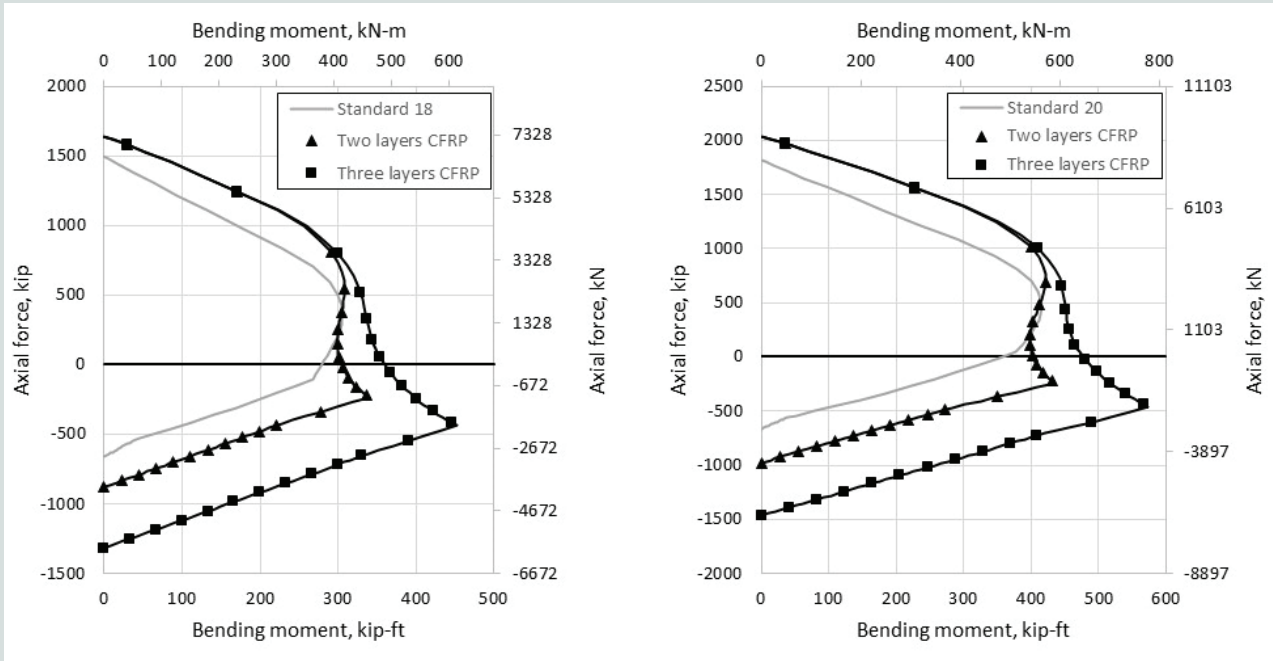
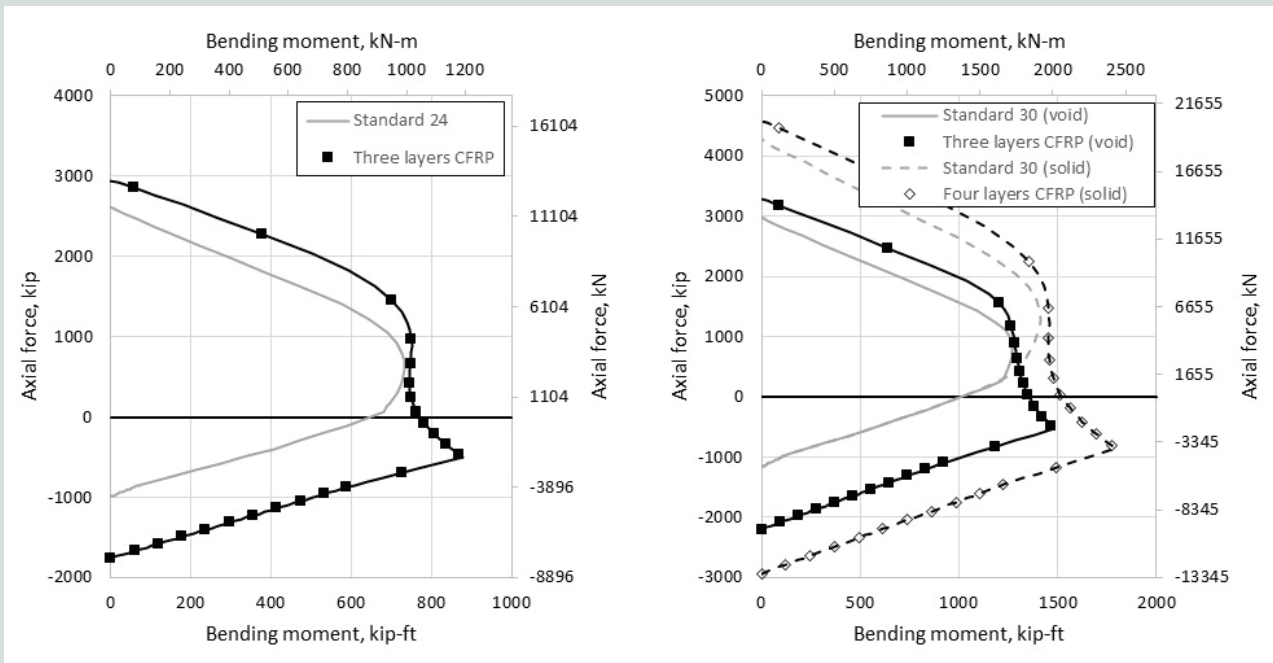


Figure 10. Interaction diagrams for carbon-fiber-reinforced polymer (CFRP) repairs of 0.3 and 0.36 m piles. Note: 1 m = 3.281 ft.



**Figure 11.** Interaction diagrams for carbon-fiber-reinforced polymer (CFRP) repairs of 0.46 and 0.51 m piles. Note: 1 m = 3.281 ft.



**Figure 12.** Interaction diagrams for carbon-fiber-reinforced polymer (CFRP) repairs of 0.61 and 0.76 m piles. Note: 1 m = 3.281 ft.

of the pile size to the moment of inertia. Figure 10 shows that one layer of longitudinally aligned, uniaxial CFRP restores almost all capacity for 0.30 and 0.35 m (1 and 1.2 ft) piles and, depending on the actual demand, may provide sufficient resistance; two layers fully envelop the undamaged interaction diagrams. For the 0.46 and 0.51 m (1.5 and 1.7 ft) piles, two

layers nearly restore full capacity, but using three layers is more conservative (Fig. 11). Larger pile sizes may or may not contain an internal void, which, depending on the final installation position, could fall within a damaged region. The 0.6 m (2 ft) and voided regions of a 0.76 m (2.5 ft) pile need three layers but with no conservative margin (Fig. 12). The minimum number

of layers necessary to provide sufficient bending capacity can be calculated on a fractional basis; however, in the field, it is impractical to apply fractional layers of fabric (strips of material rather than full-width fabric). Furthermore, partial-width strips of fabric do not provide the same encapsulation that also arrests corrosion. Hence, integer values for the number of wrap layers are preferred.

Like the model pile repair, the repair schemes in Fig. 10, 11, and 12 assume that there is no remaining prestressing steel (that is, a chloride-contaminated-zone condition), and they use the standard FDOT Class V (38 MPa [5.5 ksi]) concrete that was used in the one-third-scale testing and numerical modeling. The pile core is assumed to be compressed by a service load of 10% of ultimate axial capacity at the time of repair. Hence, the cover replacement material, which must be formed and placed before CFRP repair material is applied, would be unstressed by dead load. **Table 6**, which uses data from *Standard Specifications for Road and Bridge Construction*,<sup>12</sup> summarizes the repair schemes in Fig. 10, 11, and 12 for the same pile sizes and gives the required CFRP strength (force) per unit width of longitudinal fibers. These repairs meet or exceed the undamaged nominal capacity at any axial force (the same procedure described earlier for the one-third-scale model piles). The material is to be applied to the full perimeter of the pile sides where cover loss to spalling has been restored, which will also be discussed in part 3 of this series. Table 6 also provides the minimum number of layers using the same commercially available uniaxial carbon fiber used in the models. The computed number of required layers should be rounded up to the next integer value. No transverse confinement wrap is considered in Fig. 10, 11, or 12, but it should be included in any repair plan where the transverse FRP tensile strength is equivalent to the original steel spirals.

## Conclusion

Pile bents are a practical pier option for short-span water crossings and are easily adaptable for widening applications where

increases in traffic demands outpace service-life bridge replacement. Today, these applications are limited to designs where extreme event collision forces are unlikely; however, cycles of wetting and drying make exposed piles vulnerable to corrosion. Piles supporting water-level footings (cap and column piers) remain submerged and therefore do not experience the cycles of wetting and drying that accelerate the onset of corrosion.

When used in repairing corroded structures, FRPs have been shown to arrest the corrosion process. To restore strength, CFRP is the best choice for repairs due to the high modulus of the carbon fibers and because fewer wrap layers are required when CFRP is selected.

This study demonstrated that the design of CFRP repairs can be easily verified using off-the-shelf software already used for pier designs. The nonlinear finite element software provides user-defined cross-section modules for prestressed pile elements where prestressing levels in the strands can be tailored to match existing conditions and CFRP can be input using the additional reinforcement features. Therefore, the CFRP-repaired pile can be modeled, and the model can incorporate the exact pier geometry and soil conditions. As discussed in this paper, upper limits for bending resistance should be compared with model-predicted moments to ensure that artificially high strength gains are not unwittingly accepted directly beneath the pile cap.

This paper reports on research focused on the effects of corrosion damage on pile bent performance. Specifically, the lateral-load capacity stemming from reduced pile bending resistance is the most serious consequence of corrosion damage. The results of destructive testing on one-third-scale laboratory pile bents showed a 30% reduction in lateral capacity and a dramatic reduction in ductility when half of the prestressing steel area was lost.

Numerical modeling was shown to replicate the laboratory pile-bent loading response for damaged and undamaged

**Table 6.** Recommended longitudinal CFRP repair layers for common sizes of square piles

Pile size, m	Bending capacity, kN-m	Required CFRP, kN/mm	Number of layers (Hex103C)	Number of layers to be used
0.30	117*	1.28	1.2	2
0.36	174*	1.50	1.4	2
0.46	331	2.24	2.1	3
0.51	440	2.35	2.2	3
0.61	812	2.99	2.8	3
0.76 voided	1286	3.10	2.9	3
0.76 solid	1361*	3.63	3.4	4

Note: CFRP = carbon-fiber-reinforced polymer. 1 m = 3.281 ft; 1 kN = 0.225 kip.

\* Bending capacity is derived from calculations. All other bending capacities are from the Florida Department of Transportation's *Standard Specifications for Road and Bridge Construction*.

piles and provided a mechanism to investigate CFRP materials as a repair option. Calculations were performed and demonstrated that a single layer of CFRP wrap was predicted to fully restore the bending resistance of one-third-scale piles that had lost 100% of the steel strand area. The same calculations were used to demonstrate how production piles could also be repaired in cases where the steel prestressing strand area was lost. This approach can be easily applied to any prestressed pile size, concrete strength, or CFRP product line.

## Acknowledgments

This study was originally funded by a grant from the Florida Department of Transportation. The opinions, findings, and conclusions expressed in this publication are those of the authors and not necessarily those of the Florida Department of Transportation or the U.S. Department of Transportation.

## References

1. FDOT (Florida Department of Transportation). 2021. *Bridge Inventory 2021 Annual Report*. Tallahassee, FL: FDOT. [https://fdotwww.blob.core.windows.net/sitefinity/docs/default-source/maintenance/str/bi/annual\\_rpt\\_21.pdf?sfvrsn=7e71b1f1\\_4](https://fdotwww.blob.core.windows.net/sitefinity/docs/default-source/maintenance/str/bi/annual_rpt_21.pdf?sfvrsn=7e71b1f1_4).
2. Torres-Acosta, A. A., and A. A. Sagües. 2000. "Concrete Cover Cracking with Localized Corrosion of Reinforcing Steel." *ACI Symposium Papers*, no. 192, 591–611. <https://doi.org/10.14359/5773>.
3. Sen, R., G. Mullins, K. S. Suh, and D. Winters. 2005. "FRP Application in Underwater Repair of Corroded Piles." *ACI Symposium Papers* 230: 1139–1156. <https://doi.org/10.14359/14885>.
4. Mullins, G., R. Sen, K. Suh, and D. Winters. 2005. "Underwater Fiber-Reinforced Polymers Repair of Prestressed Piles in the Allen Creek Bridge." *Journal of Composites for Construction* 9 (2): 136–146. [https://doi.org/10.1061/\(ASCE\)1090-0268\(2005\)9:2\(136\)](https://doi.org/10.1061/(ASCE)1090-0268(2005)9:2(136)).
5. Mullins, G., R. Sen, A. Goulis, and D. Winters, D. 2025. "Lateral Capacity and Repair of Corrosion-Damaged Pile Bents, Part 1: Design and Testing Considerations." *PCI Journal* 70 (2): 56–75. <https://doi.org/10.15554/pcij70.2-02>.
6. Goulis, A. 2001. "Lateral Capacity of Corrosion Damaged Pile Bents." Master's thesis, University of South Florida Department of Civil and Environmental Engineering, Tampa, FL.
7. Mullins, G., and R. Sen. 2001. *Lateral Capacity of Corroded Pile Bents*. Final report. Tallahassee, FL: FDOT.
8. FDOT Structures Design Office. 2022. *Structures Design Guidelines*. Tallahassee, FL: FDOT. <https://www.fdot.gov/structures/docsandpubs.shtm>.
9. Mullins, G., Z. Wu, K. Johnson, and R. Sen. 2018. "Post-tensioned Splice System for Precast, Prestressed Concrete Piles: Part 2, Field Implementation and Driving Spliced Pile." *PCI Journal* 63 (3): 28–40. <https://doi.org/10.15554/pcij63.3-04>.
10. ACI (American Concrete Institute). 2014. *Building Code Requirements for Structural Concrete (ACI 318-14) and Commentary (ACI 318R-14)*. Farmington Hills, MI: ACI.
11. Scott, J. 2018. "Modeling Corrosion Damage and Repair to a 3rd Scale Concrete Bridge Bent." Master's thesis, University of South Florida Department of Civil and Environmental Engineering, Tampa, FL. <https://digitalcommons.usf.edu/etd/7228>.
12. FDOT. 2022. "Section 455-7.8: Preplanned Splices." In *Standard Specifications for Road and Bridge Construction*, 574–575. Tallahassee, FL: FDOT. <https://www.fdot.gov/programmanagement/implemented/specbooks/default.shtm>.

## Notation

$d$	= diameter of the strand
$D$	= pile size
$f'_c$	= compressive strength of concrete
$\Delta$	= change in stress

## About the authors



Gray Mullins is a professor in the Department of Civil and Environmental Engineering at the University of South Florida in Tampa, Fla.



Rajan Sen is professor emeritus in the Department of Civil and Environmental Engineering at the University of South Florida.



Michael Stokes is an associate professor in the Department of Civil and Environmental Engineering at the University of South Florida.



Joseph Scott is staff engineer and president of Rarefied Earth Inc. in Tampa, Fla.

## Abstract

Pile bents are simple, relatively inexpensive piers where typically four or more piles are driven in a line and tied together with a pile cap/beam. For overwater bridges, the bending moment in piles caused by lateral loads and the unsupported pile length often controls the design. Corrosion damage of piles in the splash zone has been shown to drastically reduce lateral capacity and ductility. This reduction in pile bending resistance can go undetected under day-to-day service loads until an extreme lateral-load event occurs. This is the second of three papers that highlight the effects of corrosion damage on bridge pile bents. The first identified the magnitude of lateral capacity loss from corrosion. This paper outlines numerical modeling efforts aimed at accurately assessing the degree of capacity loss from corrosion damage and recommends suitable carbon-fiber-reinforced polymer (CFRP) repair schemes. The final paper covers the verification testing of a severely corroded pile bent repaired with CFRP.

## Keywords

Bridge piers, carbon-fiber-reinforced polymer, CFPR, corrosion damage, lateral capacity, pile bent, steel loss.

## Review policy

This paper was reviewed in accordance with the Precast/Prestressed Concrete Institute's peer-review process. The Precast/Prestressed Concrete Institute is not responsible for statements made by authors of papers in *PCI Journal*. No payment is offered.

## Publishing details

This paper appears in *PCI Journal* (ISSN 0887-9672) V. 70, No. 4, July–August 2025, and can be found at <https://doi.org/10.15554/pcij70.4-03>. *PCI Journal* is published bimonthly by the Precast/Prestressed Concrete Institute, 8770 W. Bryn Mawr Ave., Suite 1150, Chicago, IL 60631. Copyright © 2025, Precast/Prestressed Concrete Institute.

## Reader comments

Please address any reader comments to *PCI Journal* editor-in-chief Tom Klemens at [tklemens@pci.org](mailto:tklemens@pci.org) or Precast/Prestressed Concrete Institute, c/o *PCI Journal*, 8770 W. Bryn Mawr Ave., Suite 1150, Chicago, IL 60631. 